Liquid Crystals
Publication details, including instructions for authors and subscription information:
http://www.informaworld.com/smpp/title~content=t713926090

Designing bent-core nematogens towards biaxial nematic liquid crystals

Manoj Mathews[a]; Shinwoong Kang[bc]; Satyendra Kumar[b]; Quan Li[a]
[a] Liquid Crystal Institute, Kent State University, Kent, Ohio, USA [b] Department of Physics, Kent State University, Kent, Ohio, USA [c] Department of BIN Fusion Technology, Chonbuk National University, Jeonju, Korea

Online publication date: 15 January 2011

To cite this Article Mathews, Manoj , Kang, Shinwoong , Kumar, Satyendra and Li, Quan(2011) 'Designing bent-core nematogens towards biaxial nematic liquid crystals', Liquid Crystals, 38: 1, 31 — 40
To link to this Article: DOI: 10.1080/02678292.2010.524716
URL: http://dx.doi.org/10.1080/02678292.2010.524716

Liquid Crystals,
Vol. 38, No. 1, January 2011, 31–40

Taylor & Francis
Taylor & Francis Group

Designing bent-core nematogens towards biaxial nematic liquid crystals

Manoj Mathews[a], Shinwoong Kang[b,c], Satyendra Kumar[b] and Quan Li[a*]

[a]*Liquid Crystal Institute, Kent State University, Kent, Ohio, USA;* [b]*Department of Physics, Kent State University, Kent, Ohio, USA;* [c]*Department of BIN Fusion Technology, Chonbuk National University, Jeonju, Korea*

(*Received 23 August 2010; final version received 14 September 2010*)

The nematic phase occurring in bent-core (or banana-shaped) molecule systems is conducive to the occurrence of biaxial (Nb) phase due to the inherent biaxial molecular shape. The tendency of bent-core molecules to stabilise a layered (smectic) structure poses one of the difficulties in obtaining the thermotropic Nb phase. To investigate the factors favouring the formation of the nematic phase, a number of bent-core nematic liquid crystals derived from 1, 3-phenylene central bent motifs were synthesised. Results of an investigation into the influence of the nature and position of substitutions on the central core and two rigid arms as well as the type of linkage units on the occurrence and stability of the nematic phase reveal important structure–property relationships. Textural and X-ray diffraction measurements have helped us identify molecules with the potential of exhibiting the Nb phase.

Keywords: Bent-core liquid crystals; nematic phase; biaxial nematic phase

1. Introduction

Banana-shaped liquid crystals (LCs) characterised by bent molecular motifs represent a relatively new sub-class of thermotropic LCs compared with the well-known rod- or disc-shaped mesogens. Depending on the bend angle, chemical moieties, and molecular dipoles, bent-core mesogens exhibit the conventional nematic and smectic phases of rod-shaped molecules along with several novel lamellar and columnar phases [1, 2]. In particular, spontaneous symmetry breaking in the mesophases of achiral bent-core systems induces lower symmetry ferroelectric and antiferroelectric smectic phases that are otherwise observed only in chiral liquid crystalline molecules. Owing to their distinct molecular structure, unconventional mesomorphism, and a variety of technologically useful properties such as ferroelectricity, piezo- and pyro-electricity, and second-order non-linear optical activity, bent-core mesogens have attracted a great deal of interest for the past several years. A wealth of information on the structure–property relationships of different bent-core LC molecular architectures is described in the literature [3–5].

Recently, there has been a surge of interest in the nematic phases of banana mesogens at both experimental and theoretical levels. This is based on the simple argument that the nematic phase occurring in bent-core systems is more conducive to the formation of the biaxial (Nb) phase due to the biaxial molecular shape [6–9]. In the Nb phase, a much faster electro-optic response is expected compared with the conventional uniaxial (Nu) nematic, and therefore holds the potential for revolutionising the current LC display technology. Although the Nb phase was first observed in a lyotropic mixture in 1980 [10, 11], it was only in recent years that convincing experimental evidence by X-ray diffraction (XRD) [12, 13], deuterium NMR spectroscopy [14] and electro-optical characterisation [15] had been provided for the biaxiality in low molar mass banana mesogens and shortly afterward in a laterally substituted tetrapode nematogen [16–18]. Also, electric field-induced Nb phase was found recently in the nematic phase of bent-rod and banana mesogens by an electro-optical technique [19, 20]. Several molecular design strategies incorporating disc- and rod-like mesogens [21], bent-core and rod-like dimers [22], and shape-persistent V-shaped molecules [23, 24] had also been adopted in the hope of realising biaxial nematogens.

Literature survey clearly indicates that thermotropic LCs with wide temperature range Nb phase at ambient transition temperatures are rare, and the availability of such materials is crucial for further technological applications in this field. Given the wide choice of possible structural modifications without disrupting the inherent shape biaxiality, bent-core molecules are particularly attractive. Among the vast variety of banana mesogens reported so far, only a few exhibit nematic phase and they usually appear along with conventional smectic and/or banana phases. Nevertheless, some reports on banana mesogens exhibiting only the nematic phase can be

*Corresponding author. Email: qli1@kent.edu

ISSN 0267-8292 print/ISSN 1366-5855 online

DOI: 10.1080/02678292.2010.524716
http://www.informaworld.com

found in the literature [25–30]. The rarity of nematic phase in bent-core mesogens is attributed to their favoured layered organisation for steric reasons [19]. Occurrence of tilted smectic phases below the nematic phase in bent-core molecules often leads to 'cybotactic' groups in the uniaxial nematic phase, and it calls for special attention to distinguish the Nb phase from such pre-transitional fluctuations [31]. Since only a limited number of bent-core molecules are reported to exhibit Nb phase, establishing more effective material designs and expanding the number of potential biaxial nematogens are essential to achieving the goal of ambient biaxial nematic phase and to test the validity of existing theoretical ideas. In this report, we discuss the subtle dependence of mesophase/nematic phase occurrence on minor changes in molecular architectures of five-ring 1, 3-phenylene-based bent-core molecules. With judicious structural modifications, we were able to obtain enantiotropic bent-core mesogens exhibiting (i) N phase without any smectic phase below (i.e. direct N to Cr transition) and (ii) N phase without tilted smectic phase below (i.e. having N to SmA phase transition). We also report on preliminary results of our characterisation for phase biaxiality in these N phases by polarising optical microscopy (POM) and mesophase structure by synchrotron X-ray scattering.

2. Experimental details

2.1 Materials and methods

All starting materials, solvents and reagents were obtained from commercial sources and used as purchased. All reactions involving N, N-dicyclohexylcarbodimide (DCC) and dimethylaminopyridine (DMAP) were performed in anhydrous CH_2Cl_2 solvent under a dry atmosphere of nitrogen. Column chromatography was carried out on silica gel (60–200 mesh). Analytical thin layer chromatography (TLC) was performed on commercially coated 60 mesh F254 glass plates. ^{1}H and ^{13}C NMR spectra were recorded on a Varian Gemini 200. The chemical shifts are reported in δ (ppm) relative to tetramethylsilane as internal standard. Elemental analysis was performed by Robertson Microlet Inc. Mass spectrum was taken by Mass Spectrometry & Proteomics Facility of Ohio State University. Textures and transition temperatures were observed by optical microscopy using a Leitz polarising microscope in conjunction with a Linkam TMS temperature controller. Calorimetric measurements were performed in a Perkin Elmer DSC using indium as a standard calibration.

2.2 General synthetic procedure and characterisation data of compounds 1–15

A mixture of 1.0 equiv. of acid **5**, 1.0 equiv. of phenolic derivative **6** and 1.2 equiv of DMAP dissolved in dry CH_2Cl_2 was stirred for a couple of minutes and 1.2 equiv of DCC dissolved in dry CH_2Cl_2 was added dropwise. The reaction mixture was left stirring for 12 h at room temperature in an inert atmosphere of nitrogen. After removal of the DCU by-product by filtration, the solvent was concentrated and the product was purified by column chromatography on silica with the appropriate mixture of solvents. Further recrystallisations from ethanol-CH_2Cl_2 solvent mixture afforded pure compound in 50–60% yield.

2.2.1 Data for 1

^{1}H NMR ($CDCl_3$): δ 8.38 (s, 1H, -CH=N-), 8.15–7.84 (m, 9H, ArH), 7.41–7.18 (m, 10H, ArH), 2.79–2.65 (m, 7H, Ar-CH_3, 2×Ar-CH_2), 1.67–1.14 (m, 32H, -CH_2), 0.89 (m, 6H, 2×-CH_3). ^{13}C NMR ($CDCl_3$): δ 165 .8, 164.9, 159.3, 153.7, 152.8, 152.5, 150.9, 150.5, 149.7, 146.7, 134.5, 133.8, 130.3, 130.1, 129.9, 129.1, 128.7, 128.0, 126.7, 126.4, 123.9, 122.9, 122.4, 122.3, 122.2, 36.1, 35.9, 31.9, 31.8, 31.3, 31.1, 29.7, 29.6, 29.5, 29.4, 29.3, 29.2, 29.1, 22.7, 22.6, 15.3, 14.1; HRMS: m/z calcd for $C_{54}H_{65}N_3O_4Na$ (M+Na): 842.4873. Found: 842.4885. Elemental analysis calcd for $C_{54}H_{65}N_3O_4$: C, 79.08; H, 7.99; N, 5.12. Found: C, 78.90; H, 8.12; N, 5.16.

2.2.2 Data for 2

^{1}H NMR ($CDCl_3$): δ 8.49 (s, 1H, -CH=N-), 8.38 (s, 1H, -CH=N-), 8.11–7.96 (m, 7H, ArH), 7.38–7.18 (m, 12H, ArH), 2.68 (m, 7H, 1× Ar-CH_3, 2×Ar-CH_2), 1.66–1.58 (m, 4H, -CH_2), 1.32–1.11 (m, 28H, -CH_2), 0.88 (m, 6H, 2×-CH_3). ^{13}C NMR ($CDCl_3$): δ 165.7, 164.9, 159.3, 158.3, 153.6, 153.2, 152.5, 149.7, 149.4, 141.0, 134.6, 134.1, 133.7, 130.3, 130.1, 129.9, 129.8, 129.1, 128.7, 128.0, 126.6, 126.4, 122.3, 122.2, 120.8, 36.1, 35.5, 31.9, 31.8, 31.5, 31.1, 29.7, 29.5, 29.4, 29.3, 29.2, 29.1, 22.7, 22.6, 15.4, 14.1. HRMS: m/z calcd for $C_{55}H_{66}N_2O_4Na$ (M+Na): 841.4920. Found: 841.4941. Elemental analysis calcd for $C_{55}H_{66}N_2O_4$: C, 80.65; H, 8.12; N, 3.42. Found: C, 80.38; H, 8.37; N, 3.42.

2.2.3 Data for 3

^{1}H NMR ($CDCl_3$): δ 8.38 (s, 1H, -CH=N-), 8.31–7.98 (m, 7H, ArH), 7.41–7.10 (m, 12H, ArH), 2.68 (m, 7H, 1× Ar-CH_3, 2×Ar-CH_2), 1.62–1.56 (m, 4H, -CH_2), 1.32–1.11 (m, 22H, -CH_2), 0.88 (m, 6H, 2×-CH_3). ^{13}C

NMR ($CDCl_3$): δ 165.4, 164.9, 164.6, 159.4, 155.2, 153.7, 152.6, 149.7, 148.8, 140.6, 134.7, 133.8, 131.8, 130.3, 130.1, 129.7, 129.3, 128.7, 128.0, 127.3, 126.7, 126.4, 122.3, 122.0, 121.3, 36.1, 35.4, 31.9, 31.8, 31.5, 31.1, 29.6, 29.5, 29.4, 29.3, 29.2, 29.1, 22.6, 15.3, 14.1. HRMS: m/z calcd for $C_{52}H_{59}NO_6Na$ (M+Na): 816.4240. Found: 816.4248. Elemental analysis calcd for $C_{52}H_{59}NO_6$: C, 78.66; H, 7.49; N, 1.76. Found: C, 78.53; H, 7.77; N, 1.91.

2.2.4 Data for 4

^{1}H NMR ($CDCl_3$): δ 8.71 (s, 1H, -CH=N-), 8.13–7.83 (m, 8H, ArH), 7.53–7.31 (m, 8H, ArH), 6.92–6.86 (m, 2H, ArH), 2.69 (m, 4H, 2×Ar-CH_2), 2.51 (s, 3H, Ar-CH_3), 1.66–1.11 (m, 32H, -CH_2), 0.88 (m, 6H, 2×-CH_3). ^{13}C NMR ($CDCl_3$): δ 164.6, 164.5, 162.8, 162.7, 155.3, 152.7, 150.9, 150.6, 149.7, 147.9, 146.7, 138.9, 133.5, 131.1, 130.4, 129.1, 128.7, 128.4, 126.7, 124.0, 122.9, 122.3, 119.5, 117.1, 113.3, 110.7, 36.1, 35.9, 31.9, 31.8, 31.3, 31.1, 29.7, 29.6, 29.5, 29.4, 29.3, 29.2, 29.1, 22.6, 18.6, 14.1. HRMS: m/z calcd for $C_{54}H_{65}N_3O_5Na$ (M+Na): 858.4822. Found: 858.4839. Elemental analysis calcd for $C_{54}H_{65}N_3O_5$: C, 77.57; H, 7.84; N, 5.03. Found: C, 77.65; H, 7.89; N, 5.06.

2.2.5 Data for 5

^{1}H NMR ($CDCl_3$): δ 8.48 (s, 1H, -CH=N-), 8.15–7.78 (m, 10H, ArH), 7.41–7.31 (m, 9H, ArH), 2.69 (m, 4H, 2×Ar-CH_2), 2.47 (s, 3H, Ar-CH_3), 1.65–1.11 (m, 32H, 16×-CH_2), 0.88 (m, 6H, 2×-CH_3). ^{13}C NMR ($CDCl_3$): δ 164.8, 159.4, 153.7, 152.9, 151.3, 150.9, 150.5, 149.7, 146.7, 138.9, 133.8, 130.6, 130.3, 130.2, 129.1, 128.7, 128.0, 127.4, 126.7, 124.0, 122.9, 122.3, 119.2, 36.1, 35.9, 31.9, 31.8, 31.3, 31.1, 29.6, 29.5, 29.4, 29.3, 29.2, 29.1, 22.6, 18.3, 14.1. HRMS: m/z calcd for $C_{54}H_{65}N_3O_4Na$ (M+Na): 842.4873. Found: 842.4880. Elemental analysis calcd for $C_{54}H_{65}N_3O_4$: C, 79.08; H, 7.99; N, 5.12. Found: C, 78.87; H, 7.99; N, 5.12.

2.2.6 Data for 6

^{1}H NMR ($CDCl_3$): δ 8.49 (s, 1H, -CH=N-), 8.48 (s, 1H, -CH=N-), 8.15–7.96 (m, 7H, ArH), 7.78 (d, J = 1.4 Hz, 1H, ArH), 7.40–7.12 (m, 11H, ArH), 2.69 (m, 4H, 2×Ar-CH_2), 2.47 (s, 3H, Ar-CH_3), 1.65–1.11 (m, 32H, 16×-CH_2), 0.88 (m, 6H, 2×-CH_3). ^{13}C NMR ($CDCl_3$): δ 164.9, 164.8, 159.4, 158.3, 153.6, 153.2, 151.2, 149.7, 149.4, 141.0, 138.9, 134.1, 133.7, 130.6, 130.3, 130.2, 129.9, 129.1, 128.7, 127.8, 127.4, 126.6, 122.3, 122.2, 120.8, 119.1, 36.1, 35.5, 31.9, 31.8, 31.5, 31.1, 29.7, 29.5, 29.4, 29.3, 29.2, 29.1, 22.7, 22.6, 18.3, 14.1. MS cacld for $C_{55}H_{67}N_2O_4$ (MALDI-TOF) (M+H): 819.5101; Found: 819.5560. Elemental analysis calcd for $C_{55}H_{66}N_2O_4$: C, 80.65; H, 8.12; N, 3.42. Found: C, 80.67; H, 8.15; N, 3.46.

2.2.7 Data for 7

^{1}H NMR ($CDCl_3$): δ 8.48 (s, 1H, -CH=N-), 8.31–7.97 (m, 7H, ArH), 7.78 (d, J = 1.4 Hz, 1H, ArH), 7.41–7.10 (m, 11H, ArH), 2.70 (m, 4H, 2×Ar-CH_2), 2.65 (s, 3H, Ar-CH_3), 1.65–1.11 (m, 26H, 13×-CH_2), 0.88 (m, 6H, 2×-CH_3). ^{13}C NMR ($CDCl_3$): δ 164.9, 164.6, 164.5, 159.5, 155.1, 153.6, 151.3, 149.7, 148.7, 140.6, 139.1, 133.7, 131.8, 130.6, 130.3, 130.2, 129.3, 128.7, 127.6, 127.5, 127.4, 126.6, 122.3, 122.0, 121.3, 119.2, 36.1, 35.4, 31.9, 31.8, 31.5, 31.1, 29.6, 29.5, 29.4, 29.3, 29.2, 29.1, 29.0, 22.7, 18.3, 14.1. MS calcd for $C_{52}H_{60}NO_6$ (MALDI-TOF) (M+H): 794.4421; Found: 794.4520. Elemental analysis calcd for $C_{52}H_{59}NO_6$: C, 78.66; H, 7.49; N, 1.76. Found: C, 78.39; H, 7.32; N, 1.81.

2.2.8 Data for 8

^{1}H NMR ($CDCl_3$): δ 8.41 (s, 1H, -CH=N-), 8.18–7.82 (m, 9H, ArH), 7.45–7.20 (m, 8H, ArH), 6.98 (d, J = 8.2 Hz, 2H, ArH), 4.05 (t, J = 6.6 Hz, 2H, -OCH_2), 2.69 (t, J = 8.2 Hz, 2H, Ar-CH_2), 1.83–1.26 (m, 32H, 16×-CH_2), 0.88 (m, 6H, 2×-CH_3). ^{13}C NMR ($CDCl_3$): δ 164.5, 164.1, 163.7, 161.7, 154.1, 152.4, 151.3, 150.8, 150.6, 146.7, 133.1, 132.4, 130.8, 130.5, 129.1, 127.8, 127.4, 127.3, 124.0, 123.4, 122.9, 122.5, 122.2, 121.1, 114.4, 68.4, 35.9, 31.9, 31.8, 31.3, 29.7, 29.6, 29.5, 29.4, 29.3, 29.2, 29.1, 29.0, 26.0, 22.7, 22.6, 14.1. HRMS: m/z calcd for $C_{53}H_{62}ClN_3O_5Na$ (M+Na): 878.4276. Found: 878.4276. Elemental analysis calcd for $C_{53}H_{62}ClN_3O_5$: C, 74.32; H, 7.30; Cl, 4.14; N, 4.91. Found: C, 74.13; H, 7.54; Cl, 4.42; N, 5.02.

2.2.9 Data for 9

^{1}H NMR ($CDCl_3$): δ 8.51 (s, 1H, -CH=N-), 8.17–7.84 (m, 9H, ArH), 7.57–7.25 (m, 8H, ArH), 6.98 (d, J = 8.4 Hz, 2H, ArH), 4.04 (t, J = 6.2 Hz, 2H, -OCH_2), 2.69 (t, J = 8.0 Hz, 2H, Ar-CH_2), 1.86–1.11 (m, 32H, 16×-CH_2), 0.88 (m, 6H, 2×-CH_3). ^{13}C NMR ($CDCl_3$): δ 164.5, 163.8, 163.4, 160.6, 154.1, 152.4, 150.9, 150.6, 150.5, 146.7, 133.2, 132.4, 132.1, 131.4, 130.3, 129.6, 129.1, 126.0, 124.1, 124.0, 122.9, 122.4, 122.2, 121.2, 114.5, 68.4, 35.9, 31.9, 31.8, 31.2, 29.6, 29.5, 29.4, 29.3, 29.2, 29.1, 29.0, 26.0, 22.7, 22.6, 14.1. HRMS: m/z calcd for $C_{53}H_{62}ClN_3O_5Na$ (M+Na): 878.4276. Found: 878.4276. Elemental analysis calcd

for $C_{53}H_{62}ClN_3O_5$: C, 74.32; H, 7.30; Cl, 4.14; N, 4.91. Found: C, 74.08; H, 7.57; Cl, 4.04; N, 5.16.

2.2.10 Data for 10

^{1}H NMR ($CDCl_3$): δ 8.51 (s, 1H, -CH=N-), 8.17–7.83 (m, 9H, ArH), 7.58–7.30 (m, 8H, ArH), 6.98 (d, J = 8.3 Hz, 2H, ArH), 4.05 (t, J = 6.6 Hz, 2H, -OCH_2), 2.68 (t, J = 8.8 Hz, 2H, Ar-CH_2), 1.86–1.12 (m, 32H, 16×-CH_2), 0.88 (m, 6H, 2×-CH_3). ^{13}C NMR ($CDCl_3$): δ 164.5, 163.8, 163.4, 160.6, 154.1, 152.4, 150.9, 150.6, 150.5, 146.7, 133.2, 132.4, 132.1, 131.4, 130.3, 129.7, 129.1, 126.0, 124.1, 124.0, 122.9, 122.4, 122.2, 121.2, 114.5, 68.4, 35.9, 31.9, 31.8, 31.2, 30.8, 29.6, 29.5, 29.4, 29.3, 29.2, 29.1, 29.0, 26.0, 22.7, 22.6, 14.1. HRMS: m/z calcd for $C_{53}H_{62}ClN_3O_5Na$ (M+Na): 878.4276. Found: 878.4304. Elemental analysis calcd for $C_{53}H_{62}ClN_3O_5$: C, 74.32; H, 7.30; Cl, 4.14; N, 4.91. Found: C, 74.13; H, 7.42; Cl, 3.91; N, 4.93.

2.2.11 Data for 11

^{1}H NMR ($CDCl_3$): δ 8.30 (s, 1H, -CH=N-), 7.94–7.76 (m, 8H, ArH), 7.33–6.80 (m, 9H, ArH), 4.06 (t, J = 5.8 Hz, 2H, -OCH_2), 2.61 (m, 5H, Ar-CH_3, Ar-CH_2), 1.83–1.19 (m, 38H, 19×-CH_2), 0.81 (m, 6H, 2×-CH_3). ^{13}C NMR ($CDCl_3$): δ 165.8, 161.6, 159.2, 153.2, 152.8, 152.4, 150.9, 150.8, 150.5, 146.7, 140.0, 134.5, 134.0, 130.1, 130.0, 129.1, 128.7, 128.1, 127.1, 127.0, 126.4, 124.0, 123.7, 121.9, 120.8, 111.2, 108.6, 70.1, 35.9, 31.9, 31.2, 31.3, 29.6, 29.5, 29.4, 29.3, 28.9, 25.8, 22.7, 15.3, 14.1. HRMS: m/z calcd for $C_{57}H_{69}F_2N_3O_5Na$ (M+Na): 936.5103. Found: 936.5118. Elemental analysis calcd for $C_{57}H_{69}F_2N_3O_5$: C, 74.89; H, 7.61; F, 4.16; N, 4.60. Found: C, 74.64; H, 7.70; F, 4.28; N, 4.57.

2.2.12 Data for 12

^{1}H NMR ($CDCl_3$): δ 8.38 (s, 1H, -CH=N-), 8.04–7.87 (m, 6H, ArH), 7.63 (m, 1H, ArH), 7.41–6.83 (m, 8H, ArH), 4.14 (t, J = 6.6 Hz, 2H, -OCH_2), 2.68 (m, 5H, 1× Ar-CH_3, 1×Ar-CH_2), 1.87–1.26 (m, 38H, 19×-CH_2), 0.88 (m, 6H, 2×-CH_3). ^{13}C NMR ($CDCl_3$): δ 164.3, 161.7, 159.4, 153.5, 153.1, 152.5, 150.9, 147.8, 141.3, 139.8, 139.7, 135.1, 133.9, 130.2, 129.2, 128.6, 128.3, 127.1, 127.0, 126.5, 123.4, 122.8, 122.2, 118.3, 118.2, 111.9, 111.0, 110.9, 108.5, 70.0, 36.0, 31.9, 31.2, 29.6, 29.5, 29.4, 29.3, 29.2, 29.0, 25.8, 22.7, 15.3, 14.1. MS calcd for $C_{57}H_{68}F_4N_3O_5$ (MALDI-TOF) (M+H): 950.509. Found: 950.508. Elemental analysis calcd for $C_{57}H_{67}F_4N_3O_5$: C, 72.05; H, 7.11; F, 8.00; N, 4.42. Found: C, 72.00; H, 7.28; F, 7.76; N, 4.45.

2.2.13 Data for 13

^{1}H NMR ($CDCl_3$): δ 8.38 (s, 1H, -CH=N-), 8.13 (d, J = 8.2 Hz, 2H, ArH), 8.04–8.00 (m, 3H, ArH), 7.89 (d, J = 8.2 Hz, 2H, ArH), 7.64 (m, 1H, ArH), 7.41–7.10 (m, 9H, ArH), 2.70 (m, 7H, 1× Ar-CH_3, 2×Ar-CH_2), 1.65 (m, 4H, -CH_2), 1.31–1.26 (m, 28H, -CH_2), 0.89 (m, 6H, 2×-CH_3). ^{13}C NMR ($CDCl_3$): δ 164.90, 164.3, 159.5, 153.7, 152.5, 150.9, 150.2, 149.7, 147.8, 144.5, 141.2, 139.8, 135.1, 133.7, 130.3, 130.2, 129.2, 128.7, 128.6, 128.3, 126.6, 126.5, 123.4, 122.8, 122.3, 118.2, 111.9, 36.1, 36.0, 31.9, 31.8, 31.2, 31.1, 29.6, 29.5, 29.4, 29.3, 29.2, 29.1, 22.7, 15.3, 14.1. HRMS: m/z calcd for $C_{54}H_{64}F_2N_3O_4$ (M+H): 856.4865. Found: 856.4869. Elemental analysis calcd for $C_{54}H_{63}F_2N_3O_4$: C, 75.76; H, 7.42; F, 4.44; N, 4.91. Found: C, 75.56; H, 7.66; F, 4.20; N, 4.93.

2.2.14 Data for 14

^{1}H NMR ($CDCl_3$): δ 8.48 (s, 1H, -CH=N-), 8.06–7.88 (m, 6H, ArH), 7.79 (s, 1H, ArH), 7.62 (t, 1H, ArH), 7.42–7.32 (m, 5H, ArH), 7.16 (t, 1H, ArH), 6.81–6.67 (m, 2H, ArH), 4.03 (t, 2H, J = 6 Hz, 1× -OCH_2), 2.70 (t, 2H, 1×Ar-CH_2), 2.48 (s, 3H, Ar-CH_3), 1.82–1.21 (m, 36H, 18×-CH_2), 0.88 (m, 6H, 2×-CH_3). ^{13}C NMR ($CDCl_3$): δ 166.7, 165.1, 163.6, 162.1, 161.5, 159.6, 153.4, 151.4, 151.0, 147.8, 142.0, 139.8, 139.7, 139.5, 133.8, 133.7, 130.7, 130.2, 129.2, 127.7, 126.7, 123.4, 122.3, 119.4, 118.2, 111.9, 110.9, 109.5, 102.8, 68.9, 36.0, 31.9, 31.2, 29.6, 29.5, 29.4, 29.3, 29.2, 28.9, 25.9, 22.7, 18.3, 14.1. Elemental analysis calcd for $C_{56}H_{66}F_3N_3O_5$: C, 73.26; H, 7.25; F, 6.21; N, 4.58. Found: C, 73.00; H, 7.40; F, 6.21; N, 4.58.

2.2.15 Data for 15

^{1}H NMR ($CDCl_3$): δ 8.52 (s, 1H, -CH=N-), 8.15 (d, 2H, J = 8.8 Hz, ArH), 8.02–7.87 (m, 5H, ArH), 7.60–7.16 (m, 8H, ArH), 7.16 (t, 1H, ArH), 6.98 (d, 2H, J = 8.8 Hz, ArH), 4.03 (t, 2H, J = 6.4 Hz, 1× -OCH_2), 2.69 (t, 2H, 1×Ar-CH_2), 2.92–1.21 (m, 32H, 16×-CH_2), 0.88 (m, 6H, 2×-CH_3). ^{13}C NMR ($CDCl_3$): δ 164.5, 163.8, 161.9, 160.8, 154.1, 150.9, 150.6, 147.9, 146.4, 140.6, 139.9, 133.1, 132.4, 131.9, 130.3, 129.2, 128.2, 126.6, 124.4, 123.4, 122.4, 121.1, 118.1, 118.2, 114.4, 112.0, 68.4, 36.0, 31.9, 31.8, 31.2, 29.6, 29.5, 29.4, 29.3, 29.2, 29.1, 29.0, 26.0, 22.7, 22.6, 14.1. HRMS: m/z calcd for $C_{53}H_{60}ClF_2N_3O_5Na$ (M+Na): 914.4087. Found: 914.4097. Elemental analysis calcd for $C_{53}H_{60}ClF_2N_3O_5$: C, 71.32; H, 6.78; Cl, 3.97; F, 4.26; N, 4.71. Found: C, 71.08; H, 6.78; Cl, 3.94; F, 4.29; N, 4.76.

3. Results and discussion

3.1 Materials design and synthesis

In the present study, we decided to structurally modify the bent-core mesogen **1** (A131) that had been subjected to intense investigation in recent years for biaxial order in its N phase [32–36]. Chart 1 shows the general molecular structure of 1, 3-phenylene-based target bent-core molecules (**1**–**10**) and their lateral fluoro-substituted derivatives (**11** and **15**). All molecules have substituted 3-aminobenzoic acid as an unsymmetrical 1, 3-phenylene central bent motif. The first set of molecules **1**–**3** is derived from methyl ($-CH_3$) substituted (at position Z) core by varying the linking group (L) on one of the banana arms (azo ($-N{=}N-$) group for **1**, imino ($-C{=}N-$) group for **2** and an ester ($-COO-$) group for **3**). For molecule **4**, the methyl-substituted angular central unit was modified by lateral (Y) hydroxyl ($-OH$) substitution. The effect of change in the position of $-CH_3$ substitution at the angular unit (Z′) was investigated by synthesising compounds **5**–**7**. Not only the position of substitution but also the type of molecular substitutions at the angular unit is important in determining the mesophase sequence and the associated transition temperatures. Therefore, apart from the methyl-substituted molecules, we also investigated the influence of chloro (-Cl) substitution at Z, Z′ and Z″ positions through target molecules **8**–**10**. Substitution of fluorine atom in LC bent-core molecules is well known to bring about remarkable modifications to the melting point, transition temperatures, mesophase morphology and other physical parameters [37]. In this study, we considered the fluoro substitutions in the 'arms' of the banana-shaped molecules (**11**–**15**) and compared their mesomorphic properties with non-fluorinated analogue compounds.

All the target compounds were prepared using a general synthesis pathway as shown in Scheme 1. The aldehyde **3**, obtained by DCC coupling of 4-n-alkyl/alkyloxy benzoic acid **1** with 4-hydroxybenzaldehyde/2,4-dihydroxybenzaldehyde, was subjected to a condensation reaction with respective central core unit **4** in boiling absolute ethanol in the presence of a few drops of acetic acid to get the key intermediate acid **5**. This acid was then esterified with **6** under DCC coupling reaction conditions to get the target bent-core compounds **1–15** in good yield. The materials were purified by column chromatography on silica gel followed by three times recrystallisation from ethanol-CH_2Cl_2 solvent mixture. The molecular structure and purity of all the compounds were determined by ^1H and ^{13}C NMR spectroscopy, high-resolution mass spectroscopy, and elemental analysis.

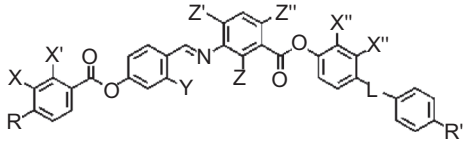

Compd.	R	X	X'	X''	Y	Z	Z'	Z''	L	R
1	C_8H_{17}	H	H	H	H	CH_3	H	H	N=N	$C_{12}H_{25}$
2	C_8H_{17}	H	H	H	H	CH_3	H	H	C=N	$C_{12}H_{25}$
3	C_8H_{17}	H	H	H	H	CH_3	H	H	COO	$C_{12}H_{25}$
4	C_8H_{17}	H	H	H	OH	CH_3	H	H	N=N	$C_{12}H_{25}$
5	C_8H_{17}	H	H	H	H	H	CH_3	H	N=N	$C_{12}H_{25}$
6	C_8H_{17}	H	H	H	H	H	CH_3	H	C=N	$C_{12}H_{25}$
7	C_8H_{17}	H	H	H	H	H	CH_3	H	COO	$C_{12}H_{25}$
8	OC_8H_{17}	H	H	H	H	Cl	H	H	N=N	$C_{12}H_{25}$
9	OC_8H_{17}	H	H	H	H	H	Cl	H	N=N	$C_{12}H_{25}$
10	OC_8H_{17}	H	H	H	H	H	H	Cl	N=N	$C_{12}H_{25}$
11	$OC_{11}H_{23}$	F	F	H	H	CH_3	H	H	N=N	$C_{12}H_{25}$
12	$OC_{11}H_{23}$	F	F	F	H	CH_3	H	H	N=N	$C_{12}H_{25}$
13	C_8H_{17}	H	H	F	H	CH_3	H	H	N=N	$C_{12}H_{25}$
14	$OC_{10}H_{21}$	H	F	F	H	H	CH_3	H	N=N	$C_{12}H_{25}$
15	OC_8H_{17}	H	H	F	H	H	H	Cl	N=N	$C_{12}H_{25}$

Chart 1. General molecular structure of the target bent-core molecules.

3.2 Liquid crystalline behaviour

The mesomorphic properties of compounds **1**–**15** were studied by POM, differential scanning calorimetry (DSC) and synchrotron XRD. No attempt was made to characterise the higher-ordered smectic phases observed for some target compounds. Phase sequences and transition temperatures of all the compounds are summarised in Table 1.

Detailed mesophase characterisation of compound **1** is previously described in the literature and it stabilises N phase followed by a SmC phase and two other higher-ordered unidentified smectic phases [32]. On the other hand, the analogue compound having no methyl ($-CH_3$) substitution at the 1, 3-phenylene core exhibits only banana mesophases [38]. In the present study, except for compound **4** all other materials with the $-CH_3$ substitution at position Z were found to be mesomorphic and exhibited the nematic and/or smectic phases. The preliminary optical and textural characterisations were made using untreated clean glass slides. Textural observation was also made under homogenous and homeotropic surface conditions. Cooling of the isotropic liquid of compound **2** between clean glass plates under the polarising optical microscope showed the formation of nematic schlieren texture at 180.9°C which, on further cooling,

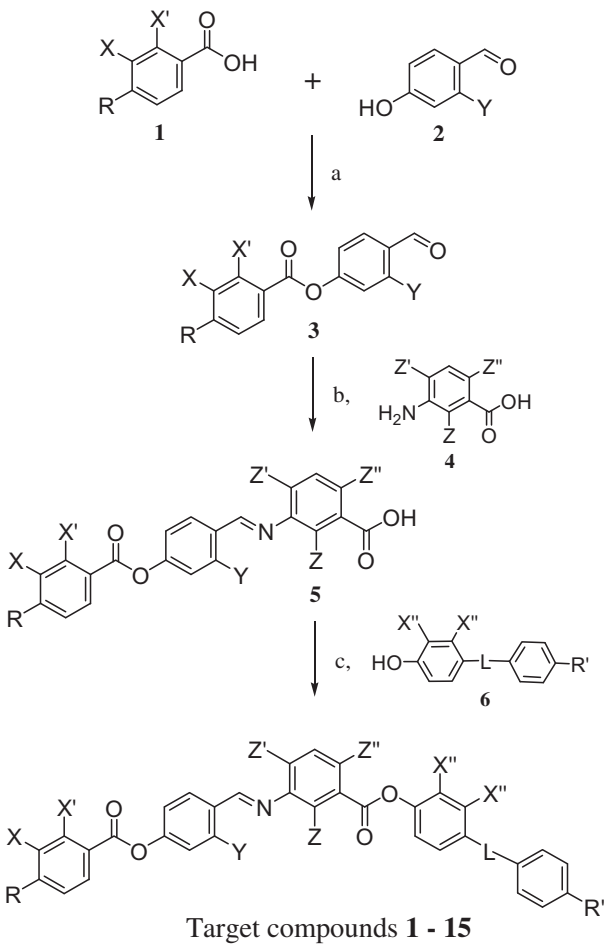

Scheme 1. General synthetic pathway used for the preparation of target bent-core molecules. (a) DCC, DMAP, CH_2Cl_2; (b) EtOH, CH_3COOH cat, reflux; (c) DCC, DMAP, CH_2Cl_2.

Table 1. Transition temperatures (°C)[a] of target banana compounds.

Compd.	Phase sequence
1	Cr 82.2 SmY 91.4 SmX 105.2 SmC 119.8 N 178.2 I I 176.5 N 118.5 SmC 104.3 SmX 85.2 SmY 55.7 Cr
2	Cr 117.9 SmY 126.4 SmX 129.8 SmC 165.0 N 182.9 I I 180.9 N 164.0 SmC 127.7 SmX 123.2 SmY 74.6 Cr
3	Cr 105.4 SmX 112.1 SmA 157.0 N 181.5 I I 180.5 N 156.1 SmA 110.4 SmX 95.6 Cr
4	Cr 136.6 I; I 96.3 Cr
5	Cr 121.0 I; I 75.2 Cr
6	Cr 128.3 I; I 97.0 Cr
7	Cr 88.6 I; I 77.8 Cr
8	Cr 83.4 SmY 119.9 SmX 125.3 SmC 141.2 N 162.9 I I 162.0 N 137.2 SmC 121.0 SmX 114.7 SmY 67.2 Cr
9	Cr 115.9 I; I 96.5 Cr
10	Cr 94.1 Bx 98.3 I; I 94.7 Bx 64.7 Cr
11	Cr 93.1 SmX 117.1 SmC 160.0 N 177.0 I I 174.8 N 157.1 SmC 110.0 SmX 81.3 Cr
12	Cr1 83.2 Cr2 97.2 SmC 130.0 N 154.7 I I 153.2 N 128.5 SmC 93.5 Cr2 55.2 Cr1
13	Cr 84.3 N 157.3 I I 155.0 N 71.1 Cr
14	Cr 107.1 I; I 81.2 Cr
15	Cr 109.3 I; I 87.2 Cr

Notes: [a]Peak temperatures in the DSC thermograms obtained during the first heating and cooling cycles at 5°C/min. Phase identified are abbreviated as Cr: crystals; N: nematic; SmA: smectic A phase; SmC: smectic C phase; SmX and SmY: unidentified smectic phases; I: isotropic liquid.

coalesced to form the planar texture. The enthalpy related to the transition from the isotropic liquid to the mesophase was 0.8 kJ/g, which is a typical value found for nematic phases. A dark field of view was obtained under homeotropic alignment conditions for this nematic phase. Further cooling to 164.0°C resulted in transition to the SmC phase as evidenced by the characteristic broken focal-conic texture under the homogenous alignment conditions. Schlieren texture was observed for the non-aligned as well as for the homeotropically aligned samples (Figure 1(a)). This compound showed two higher-ordered smectic phases (unidentified SmX and SmY) below the SmC phase before crystallising at 74.6°C. Compound **3**, with an ester linkage instead of an imine linkage on the banana arm, exhibited three enantiotropic mesophases, i.e. N, SmA and an unidentified smectic phase below the SmA phase. The planar nematic texture changed to typical SmA focal-conic texture upon cooling. Homeotropic alignment conditions produced

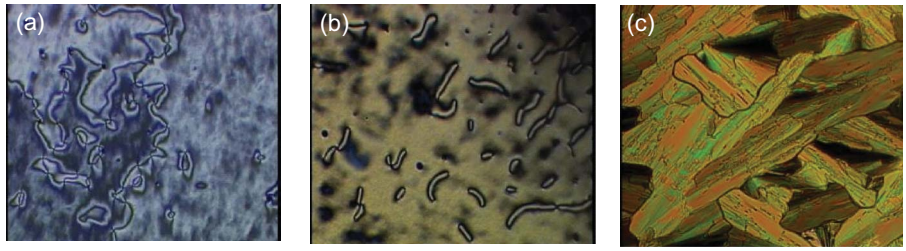

Figure 1. Optical micrographs obtained under homeotropic alignment conditions showing schlieren texture in the **SmC** phase at 125°C for compound **2** (a) and the **N** phase at 165°C for compound **3** (b). The unidentified $\mathbf{B_x}$ phase at 85°C for compound **10** between clean glass plates (c).

a schlieren texture with predominantly two-brush disclinations in the nematic phase (Figure 1(b)) while a dark field of view was obtained under crossed polarisers for the entire range of the SmA phase.

The occurrence of N phase with non-tilted SmA phase below is attractive from the view point of Nb phase characterisation. This is because the tilted smectic phases seen below the Nb phase in all of the bent-core molecules reported thus far remains a subject of debate [31]. Compound **4** with a lateral hydroxyl substitution (Y = −OH) was found to be non-mesomorphic. This we attribute to an increase in the rigidity of the molecule at the bent-core unit caused by intramolecular hydrogen bonding between the H-atom of the hydroxyl group and the N-atom of the imine functionality. Compound **5**, that differs from **1** in the position of the $-CH_3$ substitution at the 1, 3-phenylene core, was found to be non-mesomorphic. Not only **5** with azo linking unit but also **6** and **7** with imino and ester linkages, respectively, were also found to be non-liquid crystalline. Among these, compound **2** with −C=N– linking group was found to retain the mesophase sequences of the parent compound **1**, though with a reduced range for the N phase. However, an ester linking group (3) was found to induce the SmA phase below the N phase. Overall, the parent compound 1 with −N=N– linking group was found to have the widest range for the nematic phase.

Next we investigated the azo compounds **8**–**10** having a chloro (Cl) substitution at Z, Z′, or Z″ position. Compound **8** showed a similar type of textures and the mesophase sequences that were obtained for the corresponding methyl-substituted compound **1**. As can be seen, the substitution of -Cl atom reduces the isotropisation temperature by about 17°C for **8** compared with **1**, but with a reduced N-phase range. Among the other chloro derivatives, **9** was found to be crystalline while **10** exhibited an enantiotropic mesophase. The high transition enthalpy value of 16 kJ g^{-1} obtained for the isotropic to the mesophase transition for **10** is suggestive of a highly ordered banana (Bx) phase (Figure 1c).

Compounds **11** to **13** are lateral fluoro-substituted derivatives of **1** and possess $-CH_3$ substitution at position Z and an azo moiety as the linking unit (L). Compound **11**, where the fluoro substitutions are at the 'outer-ring' of the banana arm, exhibits enantiotropic N and SmC phases along with a higher-ordered unidentified phase represented as SmX. Compound **12** has fluoro substitutions on both the arms (at positions X, X′ and X″) of the molecule. Two enantiotropic phases were observed for **12**, and based on the textural observations these mesophases were identified as N and SmC phases. Interestingly, a complete suppression of the higher-ordered smectic phases were achieved in **12** compared with the non-fluorinated parent compound **1** and the fluoro-substituted derivative **11**. Compound **13** possesses a molecular structure that differs from **1** with respect to the substitution of the fluorine atom at X″ positions. Remarkably, **13** stabilises only an enantiotropic N phase. The DSC thermograms obtained for **13** during heating and cooling cycles (5°C/min) are shown in Figure 2(a). Two endothermic peaks at 84.3°C (Cr−N) and 157.3°C (N−I) on heating indicate the existence of a single mesophase. Both of these transitions are seen again during the cooling cycle. When we examined the sample between two glass plates under a POM on cooling from the isotropic liquid, nematic droplets emanate which on cooling further quickly coalesce to give marbled N texture. No change in the texture was observed until it crystallised below 72°C. Under homeotropic alignment conditions, we observed typical schlieren texture with exclusive two-brush disclinations as shown in Figure 2(b) and Figure 2(c), which is an indication of the phase biaxiality. Therefore the nematic phase of **13** was further investigated by synchrotron X-ray scattering studies. The target molecules **14** and **15** were found to be crystalline.

3.3 X-ray diffraction studies

Samples were filled in 2 mm quartz capillary and aligned by cooling from the isotropic phase in the presence of a magnetic field of approximately 2.5 kG, applied perpendicular to the X-ray beam. XRD patterns were acquired using a high-resolution image plate detector MAR-3450 placed at a distance of 541.8 mm from the sample and an X-ray wavelength of 0.7653 Å was selected. In the isotropic phase of compound **13**, the diffraction pattern consists of two diffuse rings at small and large angles. When the sample temperature was lowered into the nematic phase, the two rings condensed into two pairs of diffuse arcs along orthogonal directions (Figure 3). Thereafter, the large-angle reflections showed no qualitative change through the entire N phase. However, at lower temperatures, the small-angle arcs (corresponding to the average molecular length) fully split into two pairs of reflections. The sequence of small-angle diffraction images obtained in the nematic phase during continuous cooling from the isotropic phase for **13** is shown in Figure 4. Figure 5 shows the temperature dependence of the layer spacing, d. The changes in the shape of Bragg reflections and in the values of d clearly show two different behaviours in the N region. In the high-temperature regime, the diffraction patterns exhibit four diffuse peaks in two orthogonal directions parallel and perpendicular to the director $\boldsymbol{n}$. At low temperatures, the diffraction pattern consists of four

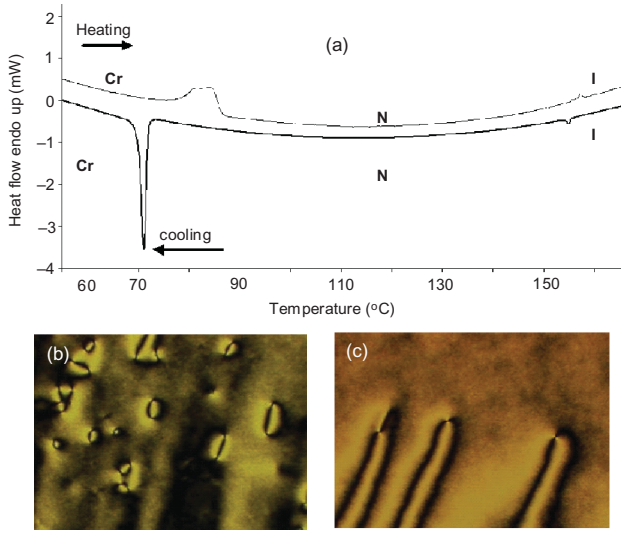

Figure 2. (a) DSC curves of first cooling and second heating of compound **13** (the scanning rate is 5°C/min). Optical micrographs obtained for compound **13** in the N phase under homeotropic alignment conditions showing schlieren texture with exclusive two-brush disclinations at 152°C (b) and at 135°C (c).

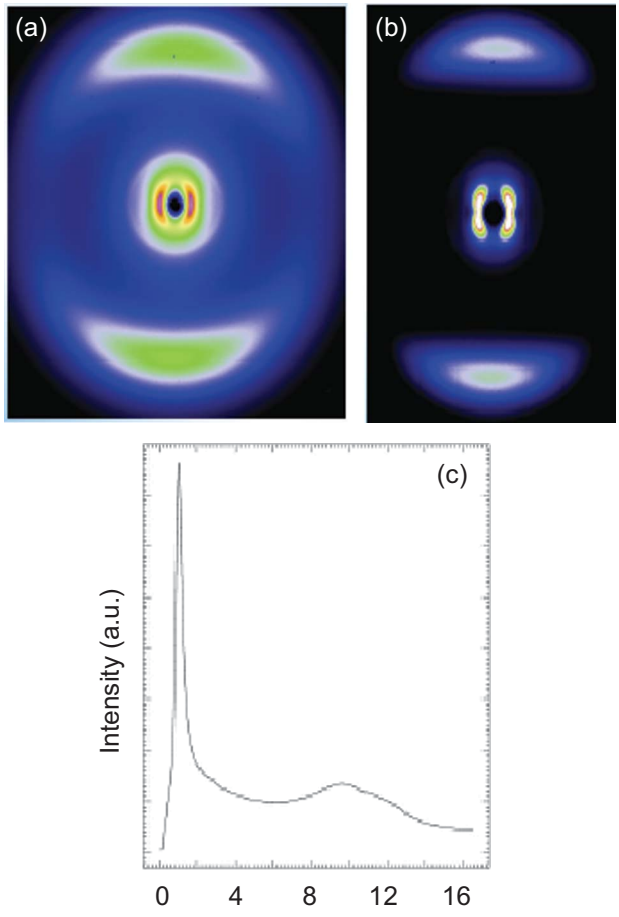

Figure 3. Large angle diffraction pattern from compound **13** in the N phase at (a) 153.8°C and (b) 74.2°C, and (c) intensity vs. diffraction angle plot obtained at 74.2°C.

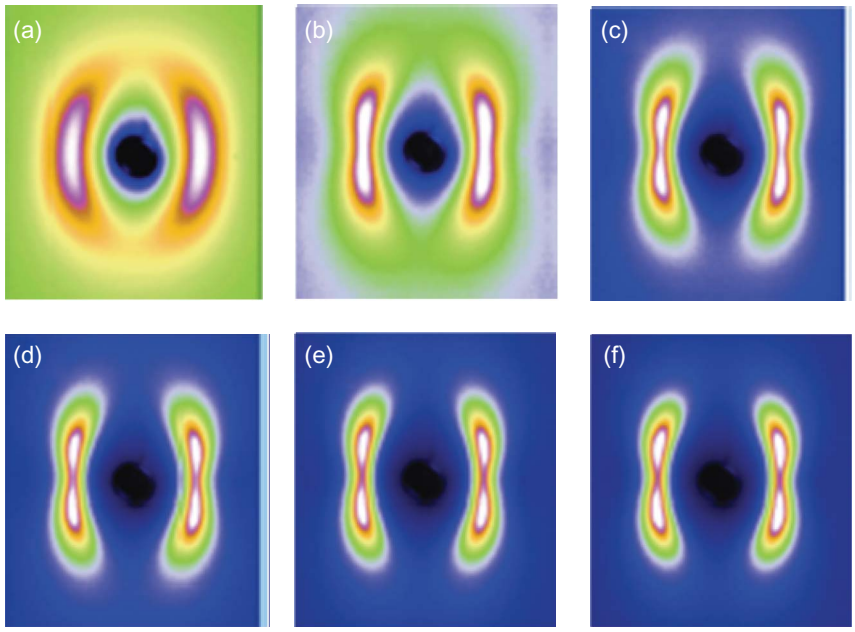

Figure 4. Small angle diffraction patterns in magnetic field aligned N phase of compound **13** during cooling at: (a) 153.8°C, (b) 125.6°C, (c) 101.9°C, (d) 92.5°C, (e) 84.0°C and (f) 74.2°C.

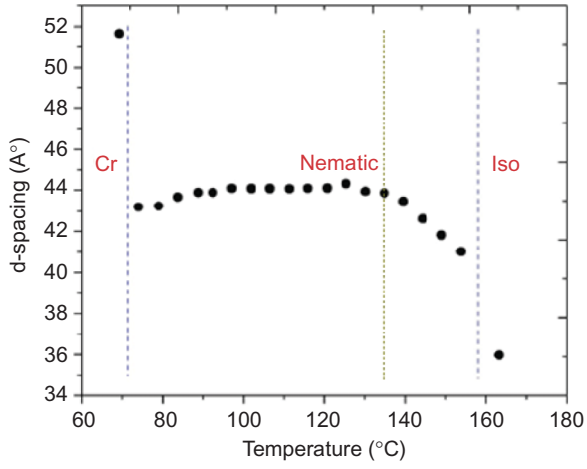

Figure 5. Layer spacing calculated from the position of the Bragg peak as a function of temperature for compound **13**.

diffused small-angle peaks and two large-angle diffuse peaks. The changes in the diffraction pattern at low temperatures may be caused by the presence of some degree of biaxiality in the N phase. However, four diffuse peaks in the uniaxial N phase of bent-core molecules can also arise from the molecular form factor or SmC-like pre-transitional fluctuations of the underlying tilted smectic phase.

It is clear that in these 1, 3-phenylene-based five-ring bent-core molecules, the type and position of the substitution at the central core unit predominantly determine the mesomorphic properties of the molecules. All the molecules that are derived from the methyl ($-CH_3$) substitution at position Z′ were found to be non-mesomorphic. Neither changing the linking groups in the arm (**5**–**7**) nor the lateral fluoro substitutions (**14**) could induce mesomorphism in these compounds. While the compounds with chloro ($-Cl$) substitution at Z and Z″, i.e. **8** and **10** are mesogenic, analogue compound **9** with substitution at Z′ was found to be non-mesomorphic. As expected, the position and the number of fluoro substituents have greatly influenced the type and the range of mesophase in these bent-core LCs.

4. Conclusion

It is a significant challenge to tune the molecular structure of the bent-core LCs to obtain nematic phases because of the tendency to stabilise smectic phases. Nevertheless, several bent-core LCs with a wide range N phase were synthesised and characterised. The structure–property relationship drawn from the current study reveals that the banana molecules that are non-symmetric at the central angular core, banana arms and terminal aliphatic chain lengths tend to stabilise the N phase over a wide temperature range. The central bent-core unit and the position and nature of substitutions on it were found to be the primary factors affecting the occurrence of the N phase. The linking groups, type and positions of the lateral substitutions on the banana arms as well as the terminal aliphatic chain lengths were secondary

factors governing the temperature range over which the N phase exists. Among the three different linking groups studied, the azo moiety favours a wide N range compared with the ester and imine linkages. Lateral fluoro substitutions on the banana arms were found to enhance the stability of the nematic phase by suppressing the smectic phase formation. When the fluorine substitution is close to the central core (compound **13**), only N phase was stabilised, and the textural and synchrotron XRD measurements indicate the possibility of biaxial nematic order. The occurrence of the N phase accompanied with the SmA phase at lower temperatures in compound **3** is attractive for understanding the formation of the Nb phase. Detailed characterisation of the N phases of the various target compounds for the phase biaxiality by XRD and electro-optical studies are currently in progress.

Acknowledgements

The work is supported by the US Department of Energy (DOE DE-SC0001412). Use of the Advanced Photon Source (APS) was supported by the Department of Energy, Basic Energy Sciences (BES), Office of Science, under Contract No. W-31-109-Eng-38. The Midwestern Universities Collaborative Access Team's (MUCAT) sector at the APS is supported by the U.S. DOE, BES, Office of Science, through the Ames Laboratory under Contract No. W-7405-Eng-82.

References

[1] Niori, T.; Sekine, T.; Watanabe, J.; Furukawa, T.; Takezoe, H. *J. Mater. Chem.* **1996**, *6*, 1231–1233.
[2] Pelzl, G.; Diele, S.; Weissflog, W. *Adv. Mater. (Weinheim, Ger.)* **1999**, *11*, 707–724.
[3] Tschierske, C.; Dantlgraber, G. *Pramana* **2003**, *61*, 455–481.
[4] Reddy, R.A.; Tschierske, C. *J. Mater. Chem.* **2006**, *16*, 907–961.
[5] Takezoe, H.; Takanishi, Y. *Jpn. J. Appl. Phys.* **2006**, *45*, 597–625.
[6] Luckhurst, G.R. *Thin Solid Films* **2001**, *393*, 40–52.
[7] Luckhurst, G.R. *Angew. Chem. Int. Ed.* **2005**, *44*, 2834–2836.
[8] Tschierske, C.; Photinos, D.J. *J. Mater. Chem.* **2010**, *20*, 4263–4294.
[9] Mettout, B. *Phys. Rev. E: Stat., Nonlinear, Soft Matter Phys.* **2005**, *72*, 031706–1–16.
[10] Yu, L.J.; Saupe, A. *Phys. Rev. Lett.* **1980**, *45*, 1000–1003.
[11] Saupe, A.; Boonbrahm, P.; Yu, L. *J. Chem. Phys.* **1983**, *80*, 7–13.
[12] Acharya, B.R.; Primak, A.; Dingemans, T.J.; Samulski, E.T.; Kumar, S. *Pramana* **2003**, *61*, 231–237.
[13] Acharya, B.R.; Primak, A.; Kumar, S. *Phys. Rev. Lett.* **2004**, *92*, 145506–1–4.
[14] Madsen, L.A.; Dingemans, T.J.; Nakata, M.; Samulski, E.T. *Phys. Rev. Lett.* **2004**, *92*, 145505–1–4.
[15] Jang, Y.; Panov, V.P.; Kocot, A.; Vij, J.K.; Lehmann, A.; Tschierske, C. *Appl. Phys. Lett.* **2009**, *95*, 183304–1–3.
[16] Merkel, K.; Kocot, A.; Vij, J.K.; Korlacki, R.; Mehl, G.H.; Meyer, T. *Phys. Rev. Lett.* **2004**, *93*, 237801–1–4.
[17] Figueirinhas, J.L.; Cruz, C.; Filip, D.; Feio, G.; Ribeiro, A.C.; Frere, Y.; Meyer T.; Mehl, G.H. *Phys. Rev. Lett.* **2005**, *94*, 107802–1–4.
[18] Neupane, K.; Kang, S.W.; Sharma, S.; Carney, D.; Meyer, T.; Mehl, G.H.; Allender, D.W.; Kumar, S.; Sprunt, S. *Phys. Rev. Lett.* **2006**, *97*, 207802.
[19] Stannarius, R.; Eremin, A.; Tamba, M.G.; Pelzl, G.; Weissflog, W. *Phys. Rev. E: Stat., Nonlinear, Soft Matter Phys.* **2007**, *76*, 061704–1–4.
[20] Nagaraj, M.; Panarin, Y.P.; Manna, U.; Vij, J.K.; Keith, C.; Tschierske, C. *Appl. Phys. Lett.* **2010**, *96*, 011106–1–3.
[21] Kouwer P.H.J.; Mehl, G.H. *J. Am. Chem. Soc.* **2003**, *125*, 11172–11173.
[22] Yelamaggad, C.V.; Prasad, S.K.; Nair, G.G.; Shashikala, I.; Shankar Rao, D.S.; Lobo, C.V.; Chandrasekhar, S. *Angew. Chem. Int. Ed.* **2004**, *43*, 3429–3432.
[23] Lehmann, M.; Kang, S.W.; Kohn, C.; Haseloh, S.; Kolb, U.; Schollmeyer, D.; Wang, Q.B.; Kumar, S. *J. Mater. Chem.* **2006**, *16*, 4326–4334.
[24] Lehmann, M.; Kohn, C.; Kresse, H.; Vakhovskaya, Z. *Chem. Commun.* **2008,** 1768–1770.
[25] Szydlowska, J.; Matraszek, J.; Mieczkowski, J.; Gorecka, E.; Pociecha, D. *Mol. Cryst. Liq. Cryst.* **2001**, *365*, 107–115.
[26] Fodor-Csorba, K.; Vajda, A.; Jakli, A.; Slugovc, C.; Trimmel, G.; Demus, D.; Gacs-Baitz, E.; Holly, S.; Galli, G. *J. Mater. Chem.* **2004**, *14*, 2499–2506.
[27] Reddy, R.A.; Sadashiva, B.K.; Raghunathan, V.A. *Chem. Mater.* **2004**, *16*, 4050–4062.
[28] Yelamaggad, C.V.; Mathews, M.; Nagamani, S.A.; Shankar Rao, D.S.; Prasad, S.K.; Findeisen, S.; Weissflog, W. *J. Mater. Chem.* **2007**, *17*, 284–298.
[29] Keith, C.; Lehmann, A.; Baumeister, U.; Prehm, M.; Tschierske, C. *Soft Matter* **2010**, *6*, 1704–1721.
[30] Francescangeli, O.; Samulski, E.T. *Soft Matter* **2010**, *6*, 2413–2420.
[31] Vaupotic, N.; Szydlowska, J.; Kovarova, A.; Svoboda, J.; Osipov, M.; Pociecha, D.; Gorecka, E. *Phys. Rev. E: Stat., Nonlinear, Soft Matter Phys.* **2009**, *80*, 030701–1–4.
[32] Prasad, V.; Kang, S.W.; Suresh, K.A.; Joshi, L.; Wang Q.; Kumar, S. *J. Am. Chem. Soc.* **2005**, *127*, 17224–17227.
[33] Dong, R.Y.; Kumar, S.; Prasad, V.; Zhang, J. *Chem. Phys. Lett.* **2007**, *448*, 54–60.
[34] Le, K.V.; Mathews, M.; Chambers, M.; Harden, J.; Li, Q.; Takezoe, H.; Jakli, A. *Phys. Rev. E: Stat., Nonlinear, Soft Matter Phys.* **2009**, *79*, 030701–1–4.
[35] Yoon, H.-G.; Kang, S.-W.; Dong, R.Y.; Marini, A.; Suresh, K.A.; Srinivasarao, M.; Kumar, S. *Phys. Rev. E: Stat., Nonlinear, Soft Matter Phys.* **2010**, *81*, 051706–1–7.
[36] Park, M.S.; Yoon, B.-J.; Park, J.O.; Prasad, V.; Srinivasarao, M. *Phys. Rev. Lett.* **2010**, *105*, 027801.
[37] Hird, M. *Chem. Soc. Rev.* **2007**, *36*, 2070–2095.
[38] Prasad, V.; Jakli, A. *Liq. Cryst.* **2004**, *31*, 473–479.